Nano Energy 30 (2016) 252–259

Contents lists available at ScienceDirect

Nano Energy

journal homepage: www.elsevier.com/locate/nanoen

Ballistic energy conversion: physical modeling and optical characterization

Yanbo Xie[a,1,*], Diederik Bos[b,1], Mark-Jan van der Meulen[c], Michel Versluis[c], Albert van den Berg[b], Jan C.T. Eijkel[b]

[a] Key Laboratory of Space Applied Physics and Chemistry, Ministry of Education and Department of Applied Physics, School of Science, Northwestern Polytechnical University, China
[b] BIOS/Lab on a Chip Group, MESA+ Institute for Nanotechnology, University of Twente, The Netherlands
[c] Physics of Fluids Group, MESA+ Institute for Nanotechnology, University of Twente, The Netherlands

ARTICLE INFO

Keywords:
Energy conversion
Microdroplets
Optical characterization
Modeling

ABSTRACT

The growing demand for renewable energy stimulates the exploration of new materials and methods for clean energy, a process which is boosted by nanoscience and emerging nanotechnologies. Recently a high efficiency and high power density energy conversion mechanism was demonstrated through the use of jetted charged microdroplets, which fully relies on the net charges stored in the electrical double layer within a hundred nanometers of the water/gas interface, and then delivered at a metal target for converting kinetic energy to electrical energy. The method is fundamentally different from the traditional electrokinetic conversion and electrostatic generators, termed as ballistic energy conversion. It has a great potential in further applications due to the ultra-simple device design and the use of water, avoiding the challenges of new materials inventions. However, thorough theory is still lacking for both a quantitative description and an optimization of this system. Here we model and experimentally characterize the physical properties of the ballistic energy conversion system. Our model predicts the optimal working conditions of the energy harvesting including initial velocity and jet size, as well as the key performance factors including efficiency, generated target voltage, and power density. The results show that by using maximally charged droplets, an appropriate size and initial velocity of microjet, the system efficiency can be over 90%, at a generated voltage below 1 kV and a power density of at least 100 W/m^2. The combination of high efficiency, huge power density, simplicity and compactness makes the ballistic energy conversion generator a promising device for green energy conversion.

1. Introduction

The demands of renewable environmental-friendly energy urge people to find novel materials and methods for energy applications [1–6]. Nanotechnologies are one of the major boosting tools for energy harvesting by taking advantages of the advanced properties of nanomaterials and high surface to bulk ratios. Particularly important hereby is energy harvesting from ambient sources, converting the ignored energy formats such as vibrations, friction and water wave energy into electricity [7–12]. With the development of micro/nanofluidics, it has become possible to harvest (electrical) energy by manipulating physicochemical processes at very high surface to bulk ratios [13–17], such as electrohydrodynamic energy conversion [18]. The motion of aqueous liquids, such as water, along a solid surface drives the net charges distributed within a hundred nanometers from the surface, and thus can converts mechanical energy to electrical energy. Low efficiency used to limit the further development of such nanofluidic electrohydrodynamic energy conversion systems, but recently the efficiency has strongly been improved in different approaches [15,19–21]. By using a design inspired by the work of Duffin et al., we obtained nearly 50% efficiency by decelerating high speed charged droplets with a metal target [22,23], in a process we termed “ballistic energy conversion” [19]. Hereby the net charges stored at the droplet air/water interface within a hundred nanometers (the typical Debye length) are transported, instead of the classical electrohydrodynamic transport at the water/solid-wall interface. Moreover, the system makes use of an acceleration/deceleration cycle to transport charges instead of a friction-based process as in the classical electrohydrodynamic energy conversion.

In ballistic energy conversion, schematically illustrated in Fig. 1, a backing pressure pushes water through a micropore, forming a microjet [24]. Due to the Rayleigh-Plateau instability [25], the water jet breaks up into droplets, capturing net ionic charges both from the electrical double layer nearby the membrane surface and additionally

* Corresponding author.
E-mail address: ybxie@nwpu.edu.cn (Y. Xie).
[1] These authors contributed equally to this work.

http://dx.doi.org/10.1016/j.nanoen.2016.10.010
Received 20 July 2016; Received in revised form 20 September 2016; Accepted 6 October 2016
Available online 06 October 2016

Nomenclature

eff_{sys}	system efficiency	a	jet radius
eff_{kin}	efficiency in acceleration stage	v_j	jet velocity
eff_{el}	efficiency in deceleration stage	v_{dr}	Initial droplet velocity
p	applied pressure	ρ_W	water mass density
$p_{eff,\,jet}$	effective pressure for jet kinetic energy	γ	surface tension
p_S	laplace pressure	C_{dr}	air drag force coefficient
p_{vis}	pressure loss by liquid viscous	C_{el}	deceleration by E field
K	viscous coefficient	L	droplet trajectory distance
		q	charge quantity
		ε	Permittivity of air

from electrostatic induction by a metal ring downstream from the pore. The induction can be operated by placing any charged objects nearby the liquid jet, whereby the capacitor formed by the liquid jet surface is inductively charged to the opposite polarity of the charged objects. In this work, we employed a DC voltage source for the electrostatic charge induction on the droplets. No current was flowing through the voltage source, so that the induction process did not consume any energy. In addition, we have also demonstrated a self-excited charging mechanism whereby no electronic power source is needed [26]. The charged droplets are collected on a metal target, generating an electrical current and locally a high electrical potential since the current flows to ground via a connected high resistance. Describing the device from an energy perspective, first pressure (potential) energy is converted into kinetic energy by accelerating the water that forms the microjet which subsequently breaks up into droplets. Then the droplet kinetic energy is converted into electrical energy when the droplets deliver charges on a target at high electrical potential, being decelerated along their trajectory by the Coulomb forces working against the movement direction.

Our results showed excellent performance (48% efficiency and maximal 160 kW/m^2 power density), an ultra-simple device and the use of common material – water, all of which enable future application as a green power source. Although there has been some theoretical analysis on liquid jet energy conversion [19,27], the optimal performance and working conditions are still not clear and there is need for a thorough theoretical model. The creation of such a model needs a quantitative physical understanding of the charged droplet kinetics in flight. In this paper, we present a theoretical model based on an optical characterization of the conversion system and predict the most important performance characteristics when the system is operated as an energy converter.

2. Model and setup

2.1. Model

Fig. 1a gives an overview of the mechanisms of conversion and energy loss. By deducting the magnitude of the energy losses during the energy conversion process, we can estimate the theoretical upper limit of the efficiency. The conversion process is defined in two stages: 1.

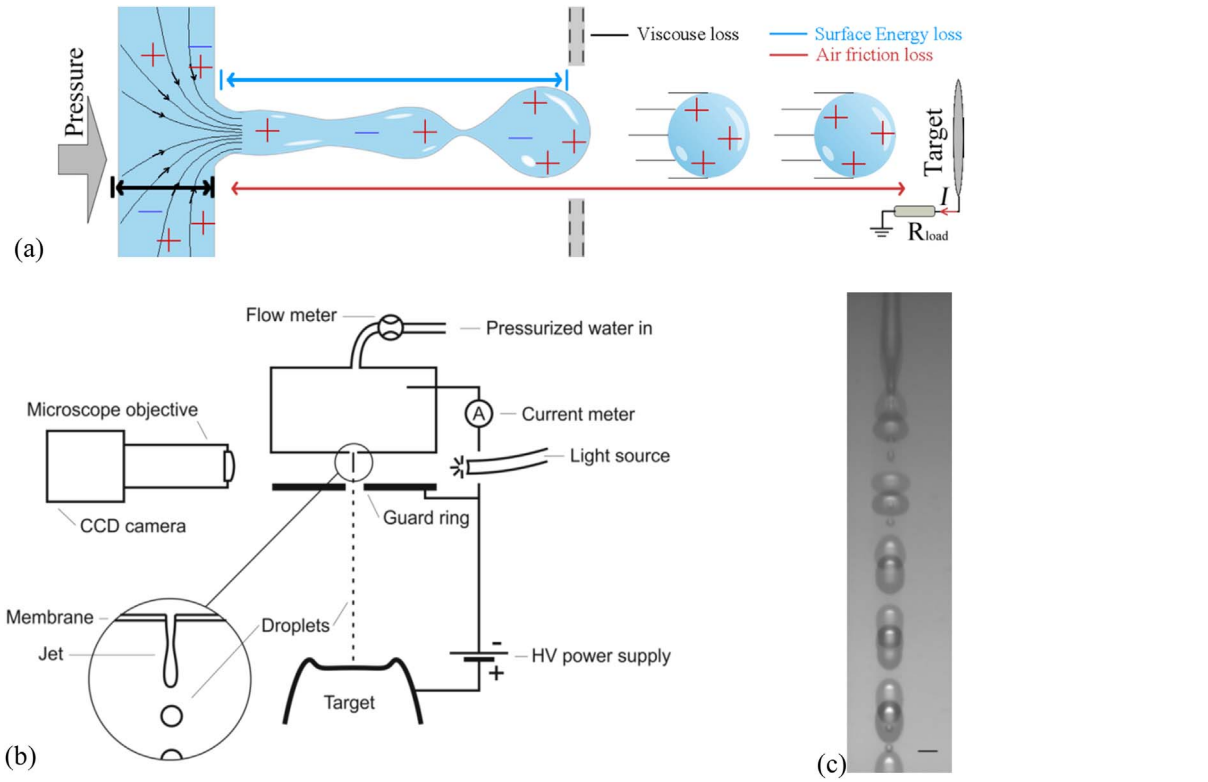

Fig. 1. (a). Energy conversion mechanisms and mechanical energy losses during the conversion process. The locations of the major energy loss factors are indicated in the schematic depicted: liquid viscous loss (black), surface energy loss (blue) and air friction loss (red). (b). Optical setup for the velocity measurements. Flow meter and water inlet are electrically isolated from the setup. (c). Sample picture by double illumination of droplets from the droplet stream from a 30 μm pore. Images are taken with 10× objective and displayed on 4.65 μm pixels. Scale bar indicates 25 μm.

Acceleration stage; the applied pressure accelerates the aqueous solution through a micropore forming a liquid microjet with an efficiency eff_{kin}. Energy is lost at this stage in form of viscous friction when the liquid is squeezed out of the micropore [28], and secondly by jet breakup into microdroplets [29]. 2. Deceleration stage; droplet kinetic energy is converted into electrical energy with an efficiency eff_{el}. The high-speed charged droplets are decelerated by the electrical field and by air friction, which we show later is the most significant loss at this stage. Finally, the overall system efficiency of ballistic energy conversion is $eff_{sys}=eff_{kin}\cdot eff_{el}$. Details on the numerical simulations of jetting can be found in Supplementary information S1. The model was validated by application to a single phase flow and showed excellent agreement with the analytical results (Supplementary information S2). In our numerical simulations we assume a monodisperse distribution of droplet size with a uniform initial speed. The role of polydispersity of the droplet size distribution and other minor factors will be discussed in the final section of this paper.

2.2. Setup and methods

The droplet speed is a key factor to quantify the energy losses in each stage. We used an optical characterization setup (Fig. 1b) to capture double-illuminated images of droplets in flight as function of several physical quantities (trajectory distance, electrical field strength, applied pressure). The droplet velocity information was extracted from the double-exposed recordings by dividing the droplet displacement by the interframe time, which typically was a few μs [30,31]. A sample image is shown in Fig. 1c. In this case (which is not typical of normal operation of the device, when the target derives its potential from the charge arriving and the load resistance) we use a high voltage source to generate the electrical target potential (*fug* - HCE 7 35000), instead of using a series resistance, to avoid the RC charging process (time delay) at the downstream circuit [19]. A dual-cavity laser source (Litron Nano-PIV Q-switched doubled Nd:YAG laser; wavelength 532 nm, 6 ns laser pulse) provides two laser pulses with 1–2 μs delay during the exposure time of the camera (Lumenera Lm135-io, 4.65 μm square pixel size). The laser is coupled into a fluorescent diffuser and the generated broadband fluorescence light remains short (~8 ns) and intense, while both the temporal and spatial coherence have been lost [32]. The incoherency makes the light pulse highly suitable for speckle-free imaging, also suppressing interference fringes. The objective lens used is connected to an Olympus BX-30MF microscope. The laser trigger time delay is controlled by a pulse/delay generator (Berkeley Nucleonics BNC 575; 250 ps accuracy).

2.3. Energy losses in the acceleration stage

The acceleration stage efficiency is defined as the ratio of the droplet kinetic power (P_{kin}) and the (input) pressure-driven mechanical power (P_{in}): $eff_{kin}=P_{kin}/P_{in}$. Two major loss factors are investigated here: energy losses due to the liquid viscous flow and the jet break up.

2.3.1. Jet formation: viscous friction and surface tension

The viscous energy loss of water flowing through an orifice can be analytically calculated using the creeping flow model known as Sampson's solution [33,34]. Alternatively, the head loss, or pressure loss, in a small opening of a circular pipe describes the viscous loss while using empirical data [35]. However, the Reynolds number in our system is close to 100, thereby breaching the creeping flow assumption, while in addition the water passing through the micropore forms a free liquid jet in air, which is fundamentally different from the liquid flow in an orifice. Hence, we used a numerical simulation of the water flow to estimate the viscous energy loss in our system.

The droplet kinetic power P_{kin} can be described as the product of the water flow rate Q and a pressure equal to the input pressure minus the pressure losses by viscous loss and Laplace pressure of the cylinder jet. We define $p_{eff,jet}$ as the effective pressure available for the kinetic energy of the liquid jet, which therefore equals the input pressure minus the pressure losses due to viscous friction, p_{vis}, and the Laplace pressure of a cylindrical jet, $p_S=\frac{\gamma}{a}$, where γ is the surface tension and a is the jet radius.

$$p_{eff,jet}=p-p_{vis}-p_S. \tag{1}$$

The viscous loss scales with the input pressure, and is inversely proportional to the jet radius a, $p_{vis}=p(\frac{K}{a})$ for laminar flow, where K is defined as the viscous loss factor.

The observed jet radius a is typically smaller than the pore radius r due to flow contraction. The contraction ratio is a complicated factor that can be influenced by pore size, shape, surface roughness and the velocity profile [36]. In experiment we observed a/r=0.9 in a 10 μm diameter pore and approximately a/r=0.8 in a 30 μm diameter pore.

The viscous loss factor K was estimated by a numerical simulation in COMSOL Multiphysics using a two-phase flow model. To exclude surface tension effects in the contraction, the surface tension of water/air in the simulations was thereby reduced by a factor of 20. Simulations then yielded a value for K of 1.30 ± 0.1 μm, determined as an average over simulations with several jet diameters ranging from 8 μm to 30 μm.

2.3.2. Jet breakup: the momentum balance

The pressure that contributes to the kinetic energy of liquid flow, $p_{eff,jet}$, given in Eq. (1), can be used to theoretically predict the flow rate Q from the Bernoulli equation. The jet velocity v_j and the flow rate Q as a function of $p_{eff,jet}$ are

$$v_j^2=\frac{2\cdot p_{eff,jet}}{\rho_w} \tag{2}$$

$$Q=\pi a^2\cdot v_j \tag{3}$$

We found that the theoretically predicted flow rate Q is in excellent agreement with our measured Q as a function of the pressure for 10 μm and 30 μm pores, as shown in Fig. 2a (red lines).

Interfacial effects influence both the flow rate from the pore (by the Laplace pressure) and the droplet breakup, as illustrated in Fig. 1a. Assuming the jet and droplets are perfectly axisymmetric, the interfacial forces are balanced in the radial (lateral) direction and the Laplace pressure reduces the net pressure exerted on the fluid, as described in Eq. (1). By conservation of mass and momentum, Schneide et al. [28] derived a relation between liquid jet and droplet velocity as:

$$v_{dr}=v_j\cdot\left(1-\frac{\gamma}{\rho_w a v_j^2}\right). \tag{4}$$

Substituting Eqs. (1) and (2) in Eq. (4) we can calculate the droplet velocity as a function of the applied pressure. The energy conversion efficiency in the accelerating stage can then be calculated as:

$$eff_{kin}=\frac{v_{dr}^2}{v_{dr,0}^2}=\left(\left(1-\frac{K}{a}\right)-\frac{\gamma}{p\cdot a}\right)\left(\frac{v_{dr}}{v_j}\right)^2, \tag{5}$$

where $v_{dr,O}$ is the velocity obtained from Bernoulli's equation in the absence of viscous losses. The first term of Eq. (5) represents the losses during jet formation, and the second term indicates the losses due to the jet breakup. Our simulated droplet velocities showed an excellent agreement with the measured droplet velocities (Fig. 2a). Fig. 2b shows that eff_{kin} increases and then saturates with increasing applied pressure. Eq. (5) can be further simplified to extract the dominant factors, consequently pointing out the way of efficiency optimization. By substituting the definition of p_{eff} ($p=\frac{p_{eff}}{eff_{kin}}=\frac{\rho_w v_j^2}{2eff_{kin}}$) and the Weber number ($We=\frac{\rho_w a v_j^2}{\gamma}$), into Eq. (5), we can rewrite $eff_{kin}=\frac{\left(1-\frac{K}{a}\right)\left(1-\frac{1}{We}\right)^2}{\frac{2}{We}\left(1-\frac{1}{We}\right)^2+1}$. We

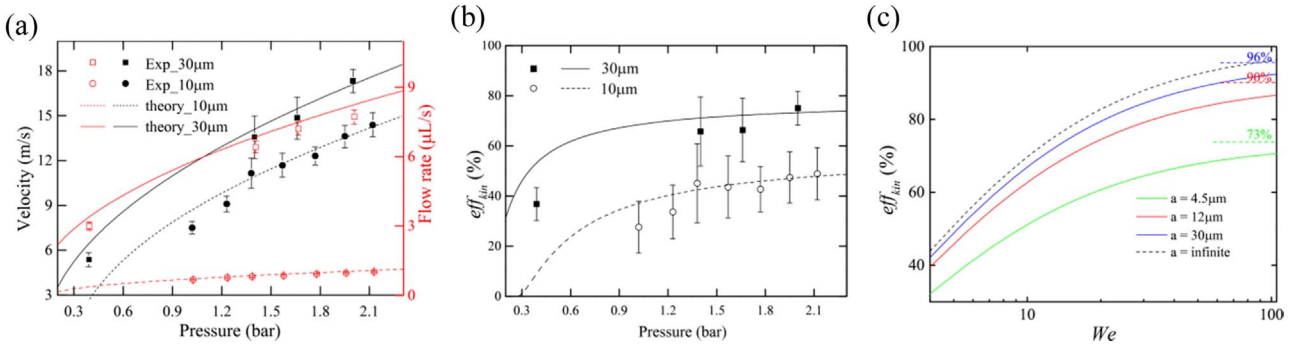

Fig. 2. Initial speed of droplets, flow rate and eff_{kin} as a function of the applied pressure. (a). Initial velocity of the droplets as a function of the applied pressure. The initial droplet velocities were measured at the position right where the jet breaks up, for 10 μm and 30 μm pores, respectively. (b) eff_{kin}, the conversion efficiency of pressure energy to droplet kinetic energy as calculated from the initial droplet velocity. The data points indicate the measured data and the lines are from Eq. (4), considering the air friction at the position of the jet breakup (calculated from Eq. (5)) in the absence of an electrical field. (c) eff_{kin} as calculated by Eq. (6): number at a given jet radius eff_{kin} (the efficiency in the acceleration stage) is only a function of the Weber.

thus find that eff_{kin} is only determined by the Weber number and the jet radius. For We $>>1$ we can further simplify to

$$eff_{kin}=\left(1-\frac{K}{a}\right)We/(2+We). \quad (6)$$

The maximal deviation between the approximation of Eq. (6) and the refined calculations is typically less than 10% for We >20 as shown in the Supplementary information S3. The results of Eq. (6) are presented in Fig. 2c for three typical jet radii. eff_{kin} increases rapidly with the Weber number, and then saturates as was observed in experiment (Fig. 2c). The theoretical upper limit of eff_{kin} can be further simplified to $eff_{kin,max}=(1-\frac{K}{a})$, when We $>>2$. The theoretical upper limit is thus only determined by the ratio of viscous loss factor and jet radius (Fig. 3b blue solid line). Finally, we can estimate the

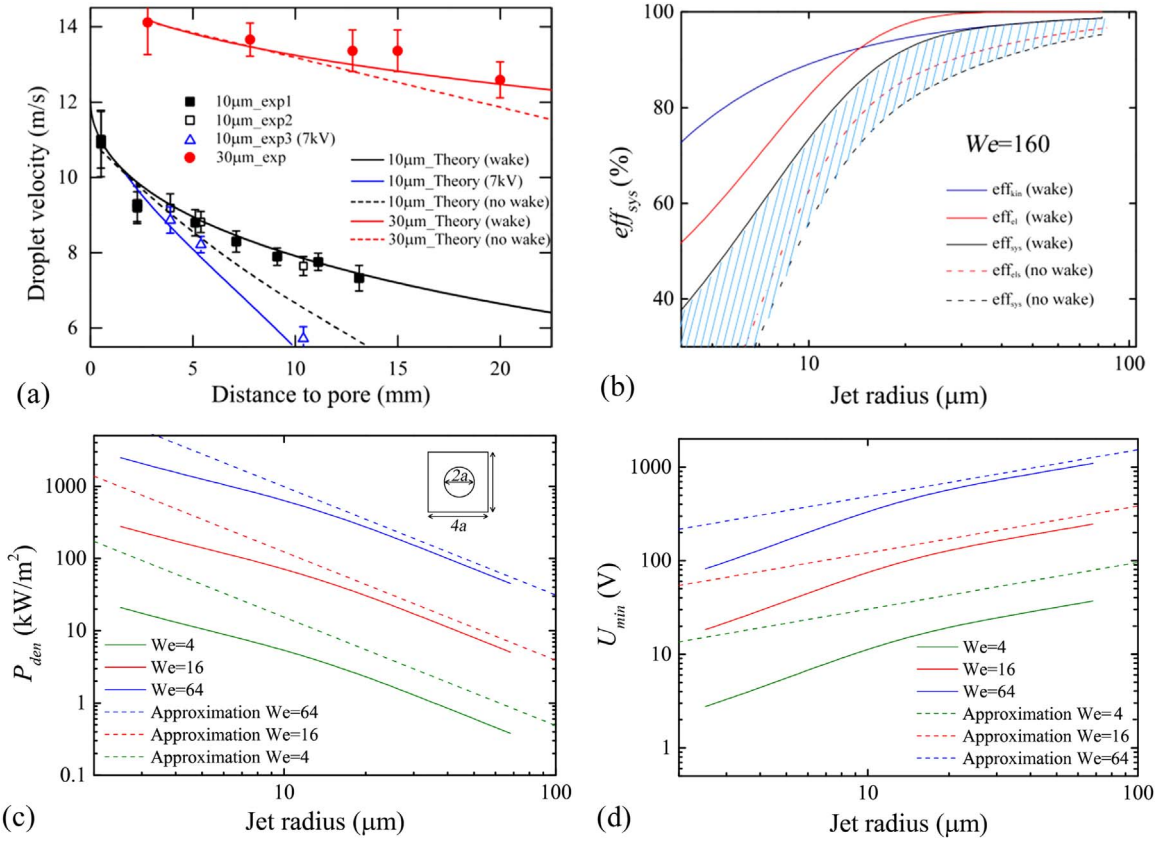

Fig. 3. The droplet velocity and the predicted energy conversion performance indicators as a function of the jet radius. (a). The droplet velocity decrease with flight distance in the absence and presence of an electrical field for a 10 μm pore (black points) and a 30 μm pore (red points) compared with two theoretical predictions, without (dashed lines) and with surrounding air motion (solid lines). The droplet velocity under 7 kV target voltage is also measured (blue triangles) and compared with our predictions (blue solid line). All experiments are operated under 1.4 bar applied pressure. In the measurements with an applied electrical field, this field was applied between 3 mm (location of the guard ring) and 13 mm (the location of the target) for a total distance L=1 cm. (b). The upper limit at high We of eff_{kin} , eff_{el} and eff_{sys} (system efficiency) as a function of the jet radius. The system efficiency increases rapidly due to a decreasing energy loss by air friction, and is dominated by viscous losses when $a>25$ μm. Both the efficiencies with (solid lines) and without (dashed lines) air wake (surrounding air flow induced by moving droplets) were calculated showing the efficiencies without any wake were overall smaller than with an air wake due to lower air friction energy losses. (c). The power density decreases with jet radius at various Weber numbers. The scaling approximation of Eq. (13) matches nicely with the calculations at large jet size. (d). The generated voltage increases with the jet radius at different Weber numbers. The major deviation between the approximation of Eq. (14) and the refined value stems from the energy loss at jet breakup ($v_j > v_{0,dr}$).

upper-limit efficiency only by a single parameter – the jet radius.

It is apparent from the above that smaller energy losses are incurred when using larger micropores, due to the smaller surface to bulk ratio dependence of both the frictional and interfacial losses. In this paper, we only consider the generation of a Rayleigh jet, where a stable liquid jet is formed producing mono-disperse droplets (see Fig. 1b). Hence, the working range of the Weber number is reported as $4 < We < 160$ with 160 the value of $0.2 \cdot \frac{\rho_W}{\rho_{air}}$ with ρ_{air} the mass density of air [30].

2.4. Energy losses in the deceleration stage

After the jet breaks up into droplets, the charged droplets are slowed down by the joint action of the electrical field and air friction. However, only the former contributes to the electrical energy conversion. The deceleration stage efficiency is defined as the ratio of the generated electrical output power (P_{out}) and the droplet kinetic power (P_{kin}): $eff_{el}=P_{out}/P_{kin}$. The single major loss factor is the energy loss due to the droplet air friction and is investigated here.

The motion of droplets during their trajectory from pore to target is described by Newton's second law:

$$m\frac{\vec{dv_{dr}}}{dt}=\vec{F_{el}}+\vec{F_{dr}} \tag{7}$$

The motion of the droplets can thus be calculated from the electric force F_{el} and the drag force F_{dr} as function of the trajectory position x.

We define a deceleration term as $C_{el}=F_{el}/m=E\rho_{el}/\rho_W$, assuming a homogeneous field, where C_{el}, E, ρ_{el}, ρ_W are the electrical deceleration, electrical field, droplet charge density and water mass density, respectively.

The air drag force on a single spherical droplet is $F_{dr}=\frac{1}{2}\rho_{air}v_{dr}^2 c_D A$, where v_{dr}, C_D, A are the speed of the droplet relative to the air, the air friction coefficient, and the projected area in the movement direction, respectively [37]. In practice, the liquid jet breaks up into a train of droplets rather than in a single droplet. This reduces the air friction on the droplets because the motion of the droplets drags the surrounding air along. Besides, more complicated effects occur: the observed downstream droplet size increases because of coalescence of the droplets in flight (see supplementary information S4); the distance between the droplets then depends on the velocity of the droplets and the occurrence of coalescence. We therefore developed a model of the air drag force and the air friction coefficient in our system, of which the parameters were obtained by fitting to experimental data and numerical simulations. It was found for the drag force that $\frac{F_{dr}}{m}=\frac{C_{dr}v_{dr}^2}{\sqrt{x}}$, where C_{dr} is an air friction coefficient, which is related to a similar boundary layer theory described by Lee [38]. The deceleration was found to scale inversely with the root of the distance from the pore, x, possibly because of the development of an air wake behind the droplets (Supplementary information S4). We numerically simulated the coefficient C_{dr} by keeping the stream of droplets stationary and moving the surrounding air. By calculating the force on the droplet surface, we obtained $C_{dr}=5.3e^{-a/5.5}$ for different jet sizes (where a is the jet radius in μm), with a maximum 7.7% deviation when the droplet radius varied from 8 μm to 20 μm and a velocity from 5 m/s to 12 m/s. With the simulated C_{dr}, we found that our calculation matched well with the experimental observations (Fig. 3a), with and without applied electrical field.

From Eq. (7), by integration we can determine the droplet velocity as a function of distance from the pore, where $v_{0,dr}$ is the initial droplet velocity just after jet breakup:

$$v^2(x)=\frac{-C_{el}}{C_{dr}}\sqrt{x}+v_{0,dr}^2 e^{-4C_{dr}\sqrt{x}}+\frac{C_{el}}{4C_{dr}^2}(1-e^{-4C_{dr}\sqrt{x}}) \tag{8}$$

In the above equation, the first term describes the velocity change due to the action of the electrical field (and thus related to the converted electrical energy), while the second and third terms represent the velocity changes due to air friction and a compensation term (stemming from the fact that friction losses decrease when more electrical energy is generated). The deceleration of microdroplets can be derived as a function of the velocity $v(x)$ from the above equation.

The kinetic energy is fully consumed when the droplets land on the target with speed equal to zero. Thus, we can obtain the maximal output power P_{out}, optimal efficiency and optimal working distance L by substituting $v(L)=0$ in Eq. (8).

The energy conversion efficiency of the deceleration stage at a distance L from the position of jet breakup can now be calculated by:

$$eff_{el}=\frac{2C_{el}L}{v_{dr,0}^2}=\frac{8LC_{dr}^2 e^{-4C_{dr}\sqrt{L}}}{-1+4C_{dr}\sqrt{L}+e^{-4C_{dr}\sqrt{L}}}. \tag{9}$$

Similar to the approach for eff_{kin}, we can simplify the efficiency in the deceleration stage to obtain the key optimization parameters. By using a Taylor expansion we can simplify Eq. (9) to

$$eff_{el}=e^{-4C_{dr}\sqrt{L}}. \tag{10}$$

The comparison of Eq. (9) and the simplified Eq. (10) is drawn in the Supplementary information S5, and shows less than 10% deviation when the jet radius is larger than 10 μm. Since $C_{dr}=5.3e^{-a/5.5}$, for a given working distance L (e.g. 1 cm) the efficiency in the deceleration stage is only determined by the jet radius. It is found that eff_{el} increases rapidly with jet size, and the air friction loss can be ignored when the jet radius is larger than 25 μm (red solid line in Fig. 3b).

As we previously reported [19], the jet forms a spray cone instead of a straight train of droplets when the droplets are highly charged, showing that repulsion forces between droplets can no longer be neglected. When moving through a wider area the droplets are more sparsely distributed, and the absence of collective wake effects leads to a higher air friction loss. To obtain the lower limit of the efficiency in the deceleration stage in the case of a spray cone, we will take an extreme (worst) case of a single droplet moving in air thus in the complete absence of a wake of leading droplets.

By solving Eq. (7), we can then derive the droplet velocity as a function of the flight distance. Similar to the case of an air wake, the efficiency of the deceleration stage for a single droplet flying in air, eff_{els}, can be described as:

$$eff_{els}=\frac{2e^{-2C_{drs}L}C_{drs}L}{1-e^{-2C_{drs}L}}, \tag{11}$$

where C_{drs} is the air friction coefficient that was derived for a single droplet. Fig. 3b (red dashed line) shows that by taking the same working distance L of 1 cm as above, eff_{els} for a single droplet is overall lower than for a train of droplets, as expected. The eff_{els} gradually increases with the jet radius because of the smaller surface to bulk ratio for large droplets.

2.5. System efficiency

By combining the equations of energy loss in the two consecutive stages, we can now predict the total system efficiency of the ballistic energy conversion

$$F_{1m} = \frac{2}{H}\int_0^H \cos\mu z \sin a_m z \, dz = 2\frac{a_m H - \mu H \sin\mu H \sin a_m H}{(a_m H)^2 - (\mu H)^2},$$

where eff_{kin} and eff_{el} are the efficiencies in the acceleration and deceleration stage by the approximate Eqs. (6) and (10). For large Weber numbers the above equation can be further simplified to:

$$eff_{sys}=\left(1-\frac{K}{a}\right)e^{-4C_{dr}\sqrt{L}} \tag{12}$$

The simplified Eq. (12) describes the theoretical upper limit of the system efficiency, which is only determined by jet size a, see Fig. 3b

(black solid line).

For the case of a droplet spray, we can estimate the system efficiency by combining Eqs. (6) and (11). The results demonstrate that about 20% additional energy is lost in a spray cone for small droplets (smaller than 10 μm) and a 5–10% energy loss occurs for large droplets. When the jet radius exceeds 70 μm, the effect of the air wake becomes negligible. With the predicted upper and lower limit of the system efficiency, the efficiencies for an arbitrary spray angle will fall within the shaded area depicted in Fig. 3b.

The above analysis seems to outline the approach of improving the energy conversion efficiency: using a high Weber number and a large jet size. However, when working with a large jet at high *We* numbers we will have a low power density and need to work at a high target voltage, which won't be the optimal conditions for energy conversion. A compromise between the different conditions thus will have to be found. We will further discuss this below.

3. Perspectives on power density and generated voltages

3.1. Power density

Here, we define the power density as the output power generated per unit area, which is a crucial factor for an energy harvesting system as it has to produce at least a reasonable power level in a small area or volume. We adopted the area of $(4\times a)^2$ as the energy generation cell, with practical micromachining restraints in mind. The power density is then given by $P_{out}/(4a)^2$. Silicon nitride membranes with large micropore arrays can be manufactured with standard cleanroom methods. We take system efficiency for the output power, giving $P_{out}=\frac{\pi}{2\sqrt{\rho_w}}(We\bullet\gamma)^{3/2}e^{-4C_{dr}\sqrt{L}}a^{1/2}$. We then obtain the power density, p_{den}:

$$P_{den} = 61.\ 2We^{3/2}\cdot a^{-3/2}\ (P_{den}: \mathrm{kW/m^2}; a: \mu\mathrm{m}) \quad (13)$$

The power density is proportional to $We^{3/2}$ which represents the input kinetic energy; it is inversely proportional to the jet radius since small droplets/jets have a higher surface to bulk ratio and hence can carry more charges.

Both the results of the refined calculations (solid lines) and the approximations (dashed lines) using the scaling laws (Eq. (13)) are shown in Fig. 3c. The scaling approximations match well with the refined calculations when the jet radius is larger than 10 μm. A high *We* helps to increase P_{den}, while a large jet size has the opposite effect. The theoretical predictions for a single jet presented above indicate a very high energy density. Ballistic energy conversion will thus have a great potential in practical use as a green energy harvesting device when a system with multiple parallel jets is created, as over 100 $\mathrm{W/m^2}$ can be obtained at the minimum velocity of the liquid jet. Multiple parallel jets can be created by using a membrane with a micromachined micropore array [39].

3.2. Generated voltage

Besides the efficiency and power density, the generated (target) voltage is also an important factor for an electrostatic generator. In our previous experiments [19], we reported on a low current-high potential system where the highest efficiencies were reached at a typical target voltage ranging from 10 to 20 kV, which is far beyond the practical levels for use in daily life, which are on the order of several hundred Volts. To minimize the target voltage, maximally charged droplets are preferable as described by the Rayleigh limit, $q_{max}=8\pi\sqrt{\varepsilon\gamma}R^{\frac{3}{2}}$, where q_{max}, γ, ε and R are the maximal charge quantity per droplet, surface tension, permittivity of air and droplet radius, respectively. Thus, the maximally generated current transported by the droplets, I_{max}, can be calculated as $I_{max}=\frac{3\pi}{2}\sqrt{\varepsilon\gamma R}\,v_j$. The maximum generated current is thus proportional to the root of the droplet radius (roughly equal to the jet radius) and the jet velocity.

By combining Eq. (12) for the system efficiency with the Rayleigh limit, we can estimate the minimum generated voltage on the target as $U_{min}=\frac{mv_{dr.0}^2}{2q_{max}}eff_{sys}$. For simplicity, we assume here that the initial droplet velocity equals the jet velocity, and that the droplet radius roughly equals the jet diameter as reported previously [30]. The minimum generated target voltage is then:

$$U_{min}=\frac{\rho_w v_j^2}{6}\sqrt{\frac{2}{\gamma\varepsilon}}a^{3/2} \quad (14)$$

Eq. (14) indicates clearly the physics behind the generated voltage U_{min}: an increase of initial droplet velocity and jet radius both increase the generated voltage through increasing the input kinetic energy; a higher surface tension of the liquid enables higher droplet charge reducing the generated voltage. The refined calculation (solid lines) and the scaling approximation of Eq. (14) (dashed lines) are shown in the Fig. 3d. The deviation between the refined calculations and approximation becomes smaller at high Weber number, as the initial droplet velocity approaches the jet velocity. Overall, when the droplets are charged to the Rayleigh limit, the generated voltage can be limited to below a kilovolt, or even to Volts.

3.3. Discussion

3.3.1. Other sources of energy loss

Besides the most significant energy losses mentioned above - liquid viscous friction, surface tension, and air friction - some other minor loss factors are discussed in this section. Here we give additional discussions of the minor energy losses based on our previous brief description [19], including electrolysis of water, droplet coalesce and corona discharge/electro-jetting. The electrolysis voltage for water (less than 2 V) is typically much smaller than the generated target voltage however can be a comparable working at the extreme case *We*=4 using 2 μm jet for the droplets charged to the Rayleigh limit. In this situation, the device seems more like a hydrogen generator other than an electricity generator. The coalesce of droplets consumes less than 2% of the kinetic energy as from our measurements [19]. But the other two minor losses can be major losses without an optimal design of the target. It is strongly recommended to make the target surface clean and smooth, without any sharp curves (can be dusts) on the target causing corona discharge or electrojetting. Besides, to minimize the loss of deflected droplets in case of a cone spray, a hemispherical target with the jet placed in the center is recommended, creating an equal flight distance for all drops in the cone.

3.3.2. Summary of the recommended working conditions

From the above discussion we find that the key performance indicators which are the efficiency, power density and generated voltage are mainly determined by the Weber number and the jet radius. However, the conditions required for high efficiency and power density and for a low generated voltage are opposite. We will here conclude and sketch working ranges of the *We* number and jet radius *a* useful for future applications.

The recommended jet radius is between 2 μm and 25 μm. Viscous losses become too large at $a < 2$ μm causing low system efficiency, while efficiency becomes nearly 100% at $a > 25$ μm so that a larger jet will not help to further increase the efficiency (Fig. 2c). The recommended Weber number for energy applications is between 4 and 78. Generating a Rayleigh jet requires $We > 4$. Increasing *We* increases the efficiency but the effect saturates when $We > 78$. A good compromise between all performance indicators is for example a device with 20 μm jet radius operated at *We*=40. Theory predicts it can maximally produce 90% efficiency for a droplet train (with surrounding air wake) or 73% efficiency for a droplet spray (entirely without air wake), 70 $\mathrm{kW/m^2}$ power density and 630 V minimum generated voltage.

4. Conclusion

We theoretically modeled and experimentally characterized the energy losses in a ballistic energy conversion system, which converts pressure-driven mechanical energy into electrical energy. The model allowed us to predict the key performance indicators of the system, efficiency, power density and generated voltage. We found that these factors depend mainly on the Weber number and jet radius. Target voltages below 1 kV can be obtained together with more than 90% system efficiency and well over 100 W/m^2 power density. Our model predicts a combination of high efficiency, high power density, and moderate voltages for the ballistic energy conversion system, which in combination with the simple construction makes it a promising device for green energy conversion.

Notes

The authors declare no competing financial interest.

Acknowledgment

Financial support of a NWO TOP (grant No. 700.58.341) (YX, AvdB, JE), the ERC (grant No. 226338-eLab4Life) (AvdB) and Fundamental Research Funds for the Central Universities (YX, No. 3102015ZY059) are gratefully acknowledged.

Appendix A. Supplementary material

Supplementary data associated with this article can be found in the online version at doi:10.1016/j.nanoen.2016.10.010.

References

[1] L. Schlapbach, A. Zuttel, Nature 414 (2001) 353–358.
[2] A.S. Arico, P. Bruce, B. Scrosati, J.M. Tarascon, W. Van Schalkwijk, Nat. Mater. 4 (2005) 366–377.
[3] Z.H. Lin, G. Cheng, L. Lin, S. Lee, Z.L. Wang, Angew. Chem. Int. Ed. 52 (2013) 12545–12549.
[4] U. Khan, T.H. Kim, H.L. Kang, J.H. Lee, H.J. Yoon, R. Bhatia, I. Sameera, W. Seung, H. Ryu, C. Falconi, Nano Energy 17 (2015) 356–365.
[5] J.H. Lee, H. Ryu, T.Y. Kim, S.S. Kwak, H.J. Yoon, T.H. Kim, W. Seung, S.W. Kim, Adv. Energy Mater. 5 (2015) 440–746.
[6] C.P. Nielsen, H. Bruus, Phys. Rev. E 89 (2014) 14.
[7] S.W. Chen, N. Wang, L. Ma, T. Li, M. Willander, Y. Jie, X. Cao, Z.L. Wang, Adv. Energy Mater. 6 (2016) 9.
[8] Z.L. Li, J. Chen, J.J. Zhou, L. Zheng, K.C. Pradel, X. Fan, H.Y. Guo, Z. Wen, M.H. Yeh, C.W. Yu, Z.L. Wang, Nano Energy 22 (2016) 548–557.
[9] H.J. Kim, J.H. Kim, K.W. Jun, J.H. Kim, W.C. Seung, O.H. Kwon, J.Y. Park, S.W. Kim, I.K. Oh, Adv. Energy Mater. 6 (2016).
[10] S.H. Kwon, J. Park, W.K. Kim, Y.J. Yang, E. Lee, C.J. Han, Y.P. Si, J. Lee, Y.S. Kim, Energy Environ. Sci. 7 (2014) 3279–3283.
[11] H. Zhang, Y. Yang, Y. Su, J. Chen, C. Hu, Z. Wu, Y. Liu, C.P. Wong, Y. Bando, Z.L. Wang, Nano Energy 2 (2013) 693–701.
[12] R. Hinchet, W. Seung, S.W. Kim, ChemSusChem 8 (2015) 2327–2344.
[13] J.C.T. Eijkel, A. van den Berg, Microfluid. Nanofluid. 1 (2005) 249–267.
[14] L. Bocquet, E. Charlaix, Chem. Soc. Rev. 39 (2010) 1073–1095.
[15] S. Haldrup, J. Catalano, M.R. Hansen, M. Wagner, G.V. Jensen, J.S. Pedersen, A. Bentien, Nano Lett. 15 (2015) 1158–1165.
[16] D. Gillespie, Nano Lett. 12 (2012) 1410–1416.
[17] M.B. Andersen, H. Bruus, J.P. Bardhan, S. Pennathur, J. Colloid Interface Sci. 360 (2011) 262–271.
[18] J. Osterle, J. Appl. Mech. 31 (1964).
[19] Y.B. Xie, D. Bos, L.J. de Vreede, H.L. de Boer, M.J. van der Meulen, M. Versluis, A.J. Sprenkels, A. van den Berg, J.C.T. Eijkel, Nat. Commun. 5 (2014) 5.
[20] J. Catalano, A. Bentien, J. Power Sources 262 (2014) 192–200.
[21] S. Haldrup, J. Catalano, M. Hinge, G.V. Jensen, J.S. Pedersen, A. Bentien, ACS Nano 10 (2016) 2415–2423.
[22] A.M. Duffin, R.J. Saykally, J. Phys. Chem. C 111 (2007) 12031–12037.
[23] A.M. Duffin, R.J. Saykally, J. Phys. Chem. C 112 (2008) 17018–17022.
[24] J. Eggers, E. Villermaux, Rep. Prog. Phys. 71 (2008) 79.
[25] L. Rayleigh, Proc. R. Soc. Lond. (1879) 196–199.
[26] Y. Xie, H.L. de Boer, A.J. Sprenkels, A. Van den Berg, J.C. Eijkel, Lab Chip 14 (2014) 4171–4177.
[27] N. Schwierz, K.J. Lam, Z. Gamlieli, J.J. Tills, A. Leung, P.L. Geissler, R.J. Saykally, J. Phys. Chem. C (2016).
[28] J.M. Schneide, N.R. Lindblad, C.D. Hendrick, J.M. Crowley, J. Appl Phys. 38 (1967) 2599- & .
[29] H.E. White, Modern College Physics, van Nostrand, New York, 1948.
[30] W. van Hoeve, S. Gekle, J.H. Snoeijer, M. Versluis, M.P. Brenner, D. Lohse, Phys. Fluids 22 (2010).
[31] A. van der Bos, A. Zijlstra, E. Gelderblom, M. Versluis, Exp. Fluids 51 (2011) 1283–1289.
[32] A. van der Bos, M.J. van der Meulen, T. Driessen, M. van den Berg, H. Reinten, H. Wijshoff, M. Versluis, D. Lohse, Phys. Rev. Appl 1 (2014) 9.
[33] R.A. Sampson, Philos. Trans. R. Soc. Lond. A 182 (1891) 449–518.
[34] A. Siria, P. Poncharal, A.L. Biance, R. Fulcrand, X. Blase, S.T. Purcell, L. Bocquet, Nature 494 (2013) 455–458.
[35] J.H. Lienhard, J.H. Lienhard, J. Fluid Eng.-T Asme 106 (1984) 13–17.
[36] H.W.K. Ernest Frederick Brater, James E. Lindell, C.Y. Wei, Handbook of Hydraulics, McGraw-Hill, New York, N. Y, 1996.
[37] L. Rayleigh, C.R. Acad, Sci. Paris 156 (1913) 109.
[38] H.C. Lee, IBM, J. Res. Dev. 21 (1977) 48–51.
[39] S. Kuiper, R. Brink, W. Nijdam, G.J.M. Krijnen, M.C. Elwenspoek, J. Membr. Sci. 196 (2002) 149–157.

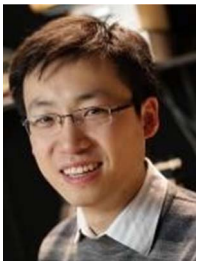

Yanbo Xie received his Master in Peking University of China in Applied Physics and Ph.D. at University of Twente in 2013. After short term stay at Huanan Normal University as a visiting scholar, he worked at Northwestern Polytechnical University as an associate Professor from 2014. He got the grant of 1000 plan for young scientist and was promoted to full professor now working at School of Science at 2015, department of Applied Physics in NPU. His research focused on the interfacial phenomena of gas/liquid/solid, including electrohydrodynamics, micro/nanofluidics in energy applications and optofluidics.

Diederik Bos (1988) received his masters degree in Electrical Engineering at Twente University in the Netherlands in 2013, with a master project on the optimization of the ballistic energy converter. At present he is employed as design engineer at ASML (Veldhoven, NL), developing diffraction-based overlay measurement applications on ASML's Yieldstar systems. His main interest is finding creative solutions for complex physics and engineering problems in the context of product development.

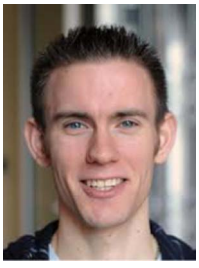

Mark-Jan van der Meulen was born on February 1st, 1986 in Apeldoorn in the Netherlands. After finishing high school in Hoogeveen in 2004 he started studying Applied Physics at the University of Twente. In 2011 he received his master's degree in the Physics of Fluids group on 3D visualization of a meniscus in piezoelectric inkjet printing. He performed his PhD research on meniscus motion and drop formation in inkjet printing in the same group and at Océ Technologies, which he defended in 2015. Currently he is active as a R & D engineer in Aero-Acoustics in the Netherlands Aerospace Center (NLR).

Michel Versluis obtained his Ph.D. degree in 1992 at the University of Nijmegen, The Netherlands, working on laser diagnostics in combustion. He continued to work on the spectroscopy of ozone-depleting molecular species, on internal combustion engines and industrial jet flames. Dr. Versluis is now full professor in the Physics of Fluids group at the University of Twente, The Netherlands. He is an expert in ultra high-speed imaging with a particular interest in the use of microbubbles and microdroplets for medical applications and in the physics and control of bubbles and droplets in microfluidic applications in medicine and the nanotechnology industry.

Albert van den Berg received his MSc in applied physics in 1983, and his Ph.D. in 1988 both at the University of Twente, the Netherlands. From 1988 to 1993 he worked in Neuchatel, Switzerland, at the CSEM. In 2000 he was appointed as full professor on Miniaturized Systems for (Bio)Chemical Analysis at the University Of Twente. In 1994 he initiated together with Prof. Bergveld the international MicroTAS conference series. He published over 400 peer reviewed publications (H=52) and received Simon Stevin award(2002), two ERC Advanced (2008, 2015) and the Spinoza prize (2009).

Jan Eijkel has a master in pharmacy at the University of Amsterdam and a Ph.D. in biosensors at the University of Twente with Piet Bergveld. After a postdoc at Imperial College London with Andreas Manz, he now is full professor Nanofluidics for Lab on a Chip Applications. Jan Eijkel is distinguished professor at South China normal University and Editor-in-Chief of Microfluidics and Nanofluidics. The focus of his research is on the investigation of physicochemical phenomena in micro- and nanofluidic systems, and their applications in Point of Care systems, including capillary phenomena, o/w two-phase flow, transport of (bio)molecules and energy generation.